Analysis of extreme ultraviolet microscopy images of patterned nanostructures based on a correlation method

P. W. Wachulak,[1,2,*] C. A. Brewer,[1,2] F. Brizuela,[1,2] C. S. Menoni,[1,2] W. Chao,[1,3] E. H. Anderson,[1,3] R. A. Bartels,[1,2] J. J. Rocca,[1,2] and M. C. Marconi[1,2]

[1]*National Science Foundation Engineering Research Center (NSF ERC) for Extreme Ultraviolet Science and Technology, Colorado State University, Fort Collins, Colorado 80523, USA*
[2]*Electrical and Computer Engineering Department, Colorado State University, Fort Collins, Colorado 80523, USA*
[3]*Center for X-Ray Optics, Lawrence Berkeley National Laboratory, Berkeley, California 94720, USA*
**Corresponding author: wachulak@lamar.colostate.edu*

Received December 21, 2007; accepted January 29, 2008;
posted February 7, 2008 (Doc. ID 90876); published April 7, 2008

A method to analyze extreme ultraviolet microscopy images of nanostructures that allows for the simultaneous determination of an object's feature size and image resolution is presented. It is based on the correlation between the image and a set of templates of known resolution generated from the original image using Gaussian filters. The analysis was applied to images obtained with a Fresnel zone plate microscope that uses a 13.2 nm wavelength laser light for illumination. The object's feature size and the resolution obtained with this method are shown to be in very good agreement with independent measurements of both magnitudes. © 2008 Optical Society of America

OCIS codes: 100.2000, 100.2960, 110.0180.

1. INTRODUCTION

The use of shorter wavelength illumination is a direct way to improve the resolution of light-based full-field microscopes. Soft-x-ray (SXR) synchrotron light has been used to demonstrate full-field zone plate microscopy with a record spatial resolution of 13 nm, an improvement factor of nearly 20 times over conventional full-field microscopes [1]. The demonstration of bright compact extreme ultraviolet (EUV) and SXR sources has made possible the development of tabletop microscopes that can render images of nanoscale objects with exposures as short as a few seconds and a spatial resolution approaching that of synchrotron-based microscopes [2–4].

The spatial resolution of an EUV/SXR microscope can be expressed in terms of the Rayleigh criterion as $R = k\lambda/\mathrm{NA}$, where λ is the wavelength of the illumination, NA is the numerical aperture of the objective zone plate, and k is a constant that depends on the coherence of the system [5]. In practice, the spatial resolution of the microscope can be assessed by analyzing images of specifically designed objects with well-established tests, such as the knife-edge or grating tests [6]. Under optimum focusing conditions, the image resolution coincides with the resolution of the imaging system.

It is straightforward to obtain the size of an object from a microscope image when it is significantly larger than the resolution limit of the instrument. However, this is not the case when the size of the object approaches the resolution limit or the image is not perfectly focused. Working at the resolution limit with objectives that have an ~100 nm depth of focus is the most common mode of operation of an EUV/SXR microscope. It is in this case that it is imperative to use robust image analysis algorithms that can identify specific object features and determine their dimensions.

Herein we present a method for the analysis of EUV and SXR microscopy images that can simultaneously extract from the image the size of the object and the resolution through a global analysis. The method makes use of the correlation between a raw EUV image and a series of templates with decreasing resolution. These templates are constructed by applying different Gaussian filters to a master binary template constructed from the original image. The analysis allows one to accurately extract the object's dimensions, even when they approach the spatial resolution of the microscope. The only required input parameter to the analysis is the microscope magnification that determines the size of the pixel in the image. The application of the method to the analysis of images obtained with a tabletop 13.2 nm wavelength laser-based microscope gives an object's dimensions that are in excellent agreement with those obtained using scanning electron microscopy (SEM) and resolution values that are consistent with those obtained by applying the Rayleigh test.

Image analysis methods are powerful tools to improve the image quality, especially in situations when noise is a dominant component [7–9]. These techniques have been successfully employed to enhance contrast in images obtained with an SXR microscope [9]. Image analysis can also be used to map the location of markers such as gold nanoparticles, commonly used in biological imaging applications [10], or to determine the position of latex nanospheres in three dimensions [11]. In general, these tools are based on a wavelet analysis. In wavelet analysis, the

resolution can be changed by factors that scale as $2^{\times}$ [12,13]. In the approach discussed herein, this limitation does not exist, and thus it allows for a more precise determination of the correlation coefficient compared to the wavelet decomposition method.

The rest of the paper is organized as follows. Section 2 briefly describes the $\lambda = 13.2$ nm microscope used to acquire the images of the periodic patterns analyzed in this paper. Section 3 discusses the image analysis method using three images obtained at high magnification as an example. Section 4 summarizes the main results. Appendix A summarizes the Gaussian filtering mathematical formalism used to analyze the images.

2. MICROSCOPY OF NANOSCALE PERIODIC PATTERNS AT $\lambda = 13.2$ nm

The EUV images used to test the correlation method described in Section 3 were acquired with a full-field microscope operating in transmission mode at a wavelength of $\lambda = 13.2$ nm [3]. Briefly, the EUV microscope uses a Fresnel zone plate (FZP) condenser and an objective with NA=0.07 and 0.132, respectively. The microscope is illuminated by the highly directional output from a $\lambda = 13.2$ nm Ni-like Cd laser operating at a repetition rate of 5 Hz [14,15]. Gratings and periodic elbow patterns fabricated by electron beam lithography on a 100 nm thick metallized silicon nitride membrane were used as test objects [16,17]. The images were recorded using a 2048 $\times$2048 back illuminated CCD camera with a 13.5 μm pixel size. Images of gratings with a 100 and 200 nm period and an elbow-shaped grating with a 100 nm period were obtained at a magnification of 1080×. At this magnification, the pixel size in the image plane corresponds to 12.5 nm at the object plane, which ensures that the image resolution is not limited by the detection system. The spatial resolution of the $\lambda = 13.2$ nm microscope was obtained from the analysis of EUV images of gratings with periods down to 76 nm [3]. Figure 1 shows the EUV images used to test the correlation method described in Section 3 and compares them with SEM images from which the linewidths of the test patterns were independently assessed.

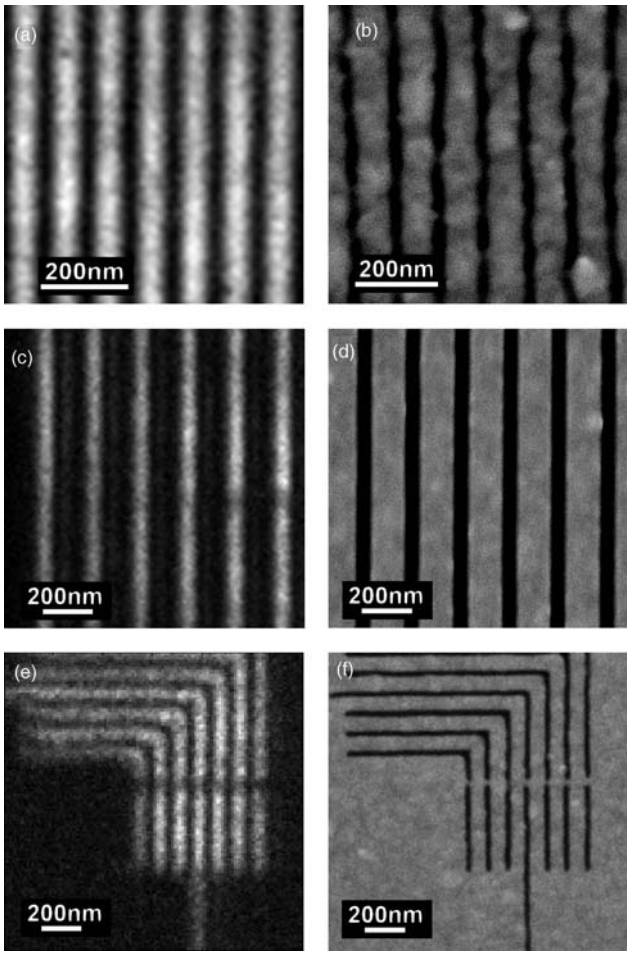

Fig. 1. EUV microscope image of (a) 100 nm full-period grating, (c) 200 nm full-period grating, and (e) 100 nm full-period elbow-shaped grating obtained with a 13.2 nm wavelength laser illumination. (b), (d), and (f) are the corresponding SEM images of the test objects.

3. ALGORITHM FOR THE SIMULTANEOUS DETERMINATION OF FEATURE SIZE AND RESOLUTION

We illustrate the sequence of steps implemented in our image analysis method utilizing the EUV image of the 200 nm full-period grating shown in Fig. 1(c). First an intensity threshold filter is applied to the raw EUV image data to homogenize the background. The threshold level is adjusted to maintain the features of the image while generating a new image with improved contrast for the next processing step. The thresholded image is shown in Fig. 2(a). In a second step a skeletonizing algorithm is applied to the thresholded image [18] to produce a template with one-pixel-wide contours that follows the shape of the original image. The skeleton of the grating of Fig. 1(c) is shown in Fig. 2(b). Third, the skeleton is convolved with K different circular templates of diameters ranging, in this particular example, from 5 to 100 nm. The convolution between the skeleton and the K different circular templates generates a set of K binary templates, each with a different linewidth, that resemble the original grating image. One of these K binary templates with a diameter of 50 nm is shown in Fig. 2(c). Fourth, the K templates are degraded in resolution by applying L different Gaussian filters with selected full width at half-maximum (FWHM). A description of the Gaussian filters' design and their relationship to the image resolution is provided in Appendix A. Figure 3 shows a set of degraded resolution templates obtained from the binary image in Fig. 2(c) after the convolution with Gaussian filters of different FWHM. In these templates the image resolution varies from 15 to 165 nm in 30 nm steps. Applying the L Gaussian filters to each one of the K binary templates produces a set of $K \times L$ templates. These $K \times L$ templates are individually correlated with the original raw image. The correlation coefficients plotted in the $K \times L$ dimensional space generate a surface whose global maximum identifies the template that best resembles the original EUV image. We associate the K- and L-indices of the template that

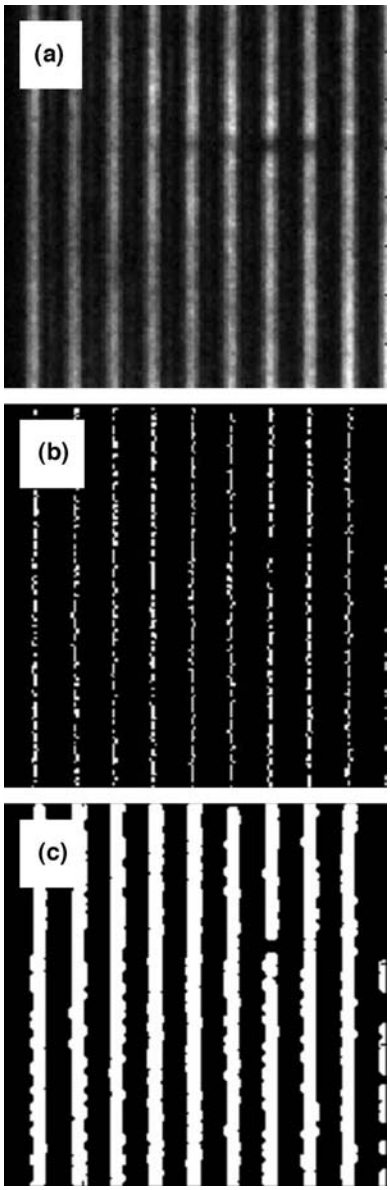

Fig. 2. (a) EUV image of the 200 nm full-period grating. (b) Skeleton obtained from the image shown in (a). (c) Binary template generated by convolution of the skeleton image with a circle with diameter $D=50$ nm.

maximize the correlation to the size of the feature and the resolution of the image, respectively.

To relate an image resolution to the microscope's Rayleigh resolution, the Gaussian filter method was applied to a set of synthesized images of two Airy disks separated by distances R and corresponding to the images from two point sources. The distance R was set equal to the Rayleigh resolution. Independently, images consisting of two pixels also separated by a distance R were degraded in resolution by applying Gaussian filters of different FWHM. Figure 4 is a plot of the resolution derived from applying the Gaussian filters with a given FWHM that maximizes the correlation value between the degraded two-pixel image and the synthesized Airy pattern image as a function of the separation R. The linear dependence indicates that both magnitudes are equivalent, and the

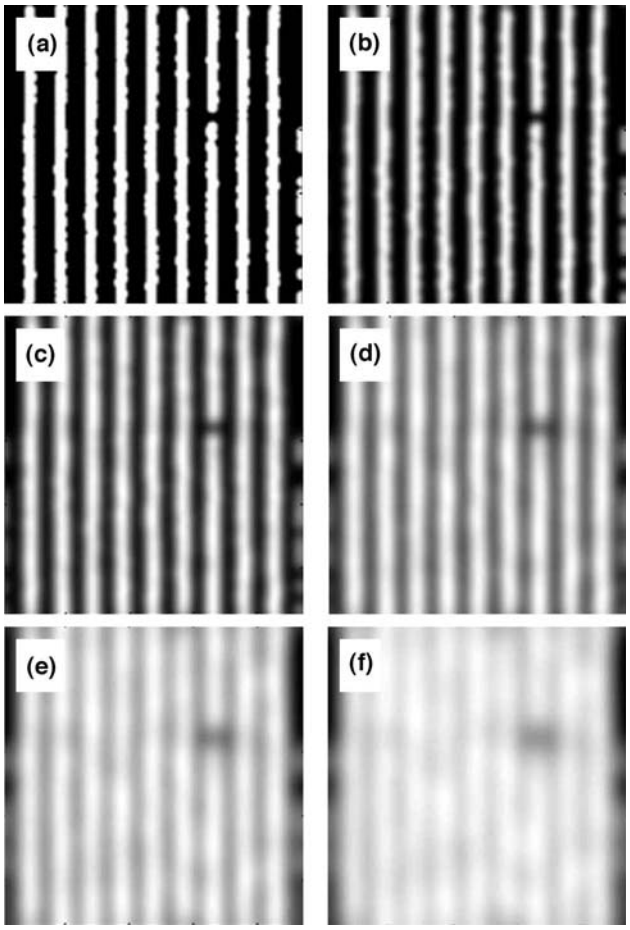

Fig. 3. Set of templates obtained applying Gaussian filters of different FWHM yielding different resolutions of δ. (a) $\delta=15$, (b) $\delta=45$, (c) $\delta=75$, (d) $\delta=105$, (e) $\delta=135$, and (f) $\delta=165$ nm.

slope is $\beta=0.786$. Therefore the image's Rayleigh resolution can be obtained by dividing the Gaussian method resolution by the factor β. A detailed explanation of the relation between the resolution and the FWHM of the Gaussian filter is given in Appendix A.

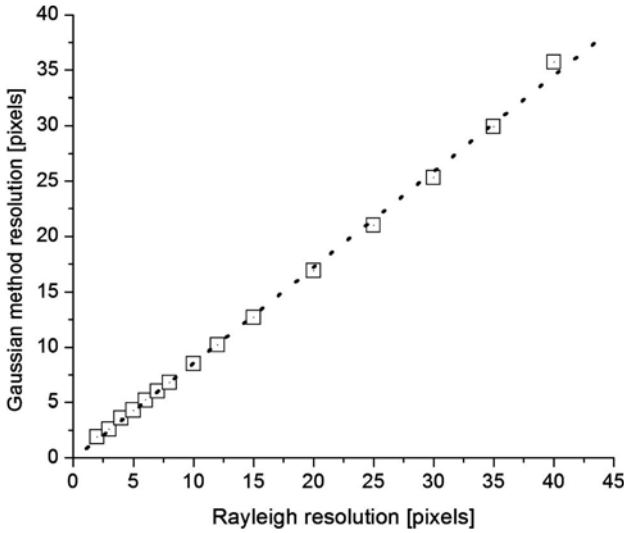

Fig. 4. Resolution derived from the optimum Gaussian filter size as a function of the Rayleigh resolution.

Figure 5 shows the correlation plots generated by applying the algorithm to the three images in Fig. 1. Each calculated point in this plot has a minimum step size in both axes of 5 nm. The smooth surface plot was obtained by bicubic interpolation. From the plots we estimated the feature size and image resolution for each pattern. The error in the image resolution was conservatively assigned to one step size used to generate the plots shown in Fig. 5, in this case 5 nm. The grating linewidths obtained for all three patterns are in very good agreement with those obtained independently from the SEM images. The error bars in the linewidths, obtained from the SEM images, correspond to the standard deviation of the values measured at ten different locations in the image. Table 1 summarizes the results. Other images containing patterns with different shapes were also analyzed, resulting in similar degrees of agreement. The Rayleigh resolution obtained from the image analysis is in agreement with the measured spatial resolution of the $\lambda = 13.2$ nm microscope that yielded a resolution better than 76 nm (38 nm half-period resolution) [3].

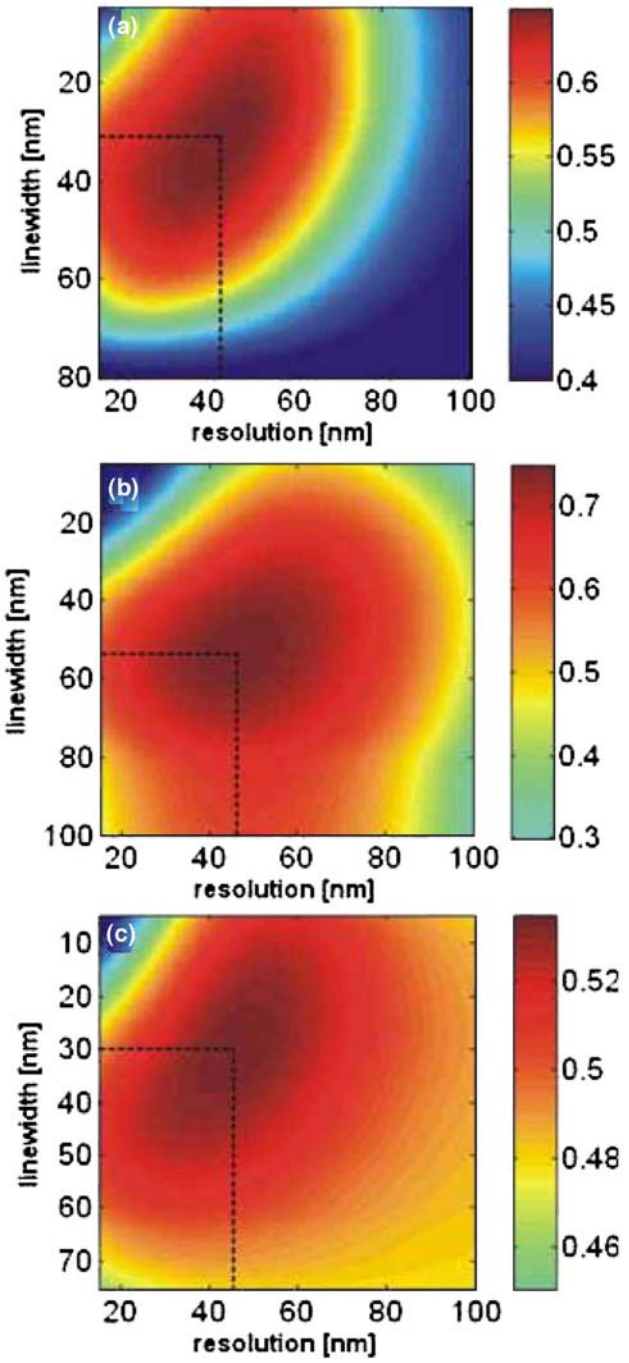

Fig. 5. (Color online) Correlation coefficients plotted in the feature size-resolution space showing a global maximum for each of the three different images in Fig. 1. The dashed lines indicate the coordinates of the global maxima for each of the data sets: (a) 100 nm full-period grating linewidth 31±5 nm and resolution 54.8±5 nm; (b) 200 nm full-period grating, linewidth 53.6±5 nm, and 59.2±5 nm resolution; and (c) 100 nm full-period elbow-shaped grating, linewidth 29±5 nm, and 58.3±5 nm resolution.

4. CONCLUSIONS

We have demonstrated a correlation method that is capable of simultaneously determining the size of the imaged features and the resolution of a full-field EUV microscope image. Its global approach makes the method robust and tolerant of local variations in image contrast. The method was applied to determine the size of nanoscale patterns from images of patterned nanostructures acquired with a 13.2 nm wavelength and a FZP microscope. The results obtained are in very good agreement with independent measurements of both magnitudes. Image analysis algorithms that evaluate the image resolution, such as the one described here, have the capability to enable the optimization of the EUV/SXR microscope during image acquisition. This is especially critical for the acquisition of EUV images with high-NA zone plates, where depth of focus is limited to ~100 nm or less.

APPENDIX A: DESCRIPTION OF THE DESIGN OF THE GAUSSIAN FILTERS AND THEIR RELATION TO THE IMAGE RESOLUTION

The method used to estimate the image resolution is based on the correlation between the raw image and a series of synthesized templates of known feature size and resolution that are generated by appropriate processing of the original image as described in Section 3.

The image and templates are digital in nature and therefore pixelated. They can be considered as a discrete version of a continuous image $c(x,y)$ sampled in a matrix. If we assume a grid of $M \times N$ pixels in size w_x and w_y, the sampled image $c(x_m,y_n)$ is obtained by multiplication of $c(x,y)$ with an array of delta functions located in every pixel,

$$c(x_m,y_n) = \sum_{m \in M} \sum_{n \in N} \delta(x - x_m, y - y_n) \cdot c(x,y), \qquad \text{(A1)}$$

where $x_m = w_x \cdot m$ and $y_n = w_y \cdot n$ are the coordinates of the pixel (m,n).

The pixelated image can be represented as a convolution between the sampled image $c(x_m,y_n)$ with a two-dimensional (2D) rectangular function $p(w_x,w_y)$ that represents the pixel.

Table 1. Comparison of the Results in Linewidth and Image Resolution Obtained by the Correlation Algorithm with Independent Methods for Three Different Images Obtained with the EUV Microscope and 13.2 nm Illumination

	Test Image		
	100 nm Period Gratings (nm)	200 nm Period Gratings (nm)	100 nm Period Elbow-Shaped Gratings (nm)
Grating linewidth SEM measurements	31±2.6	53.8±1.8	31.3±2.4
Grating linewidth from the algorithm	31±5	53.6±5	29±5
Image resolution determined by algorithm (δ/β)	54.8±5	59.2±5	58.3±5
Instrument resolution from grating test measurement	<76	<76	<76

The first of the reference templates is binary, i.e., the function $c(x_m,y_n)$ has only two possible values, 0 or 1. With this assumption the binary template can be expressed as

$$i_b(x,y) = c_b(x_m,y_n) \otimes p(w_x,w_y) = \left[\sum_{m\in M}\sum_{n\in N}\delta(x-x_m,y-y_n)\cdot c_b(x,y)\right] \otimes p(w_x w_y), \tag{A2}$$

where $c_b(x_m,y_n)$ is a binary function that represents the sampled binary image. In the spatial frequency domain the function $p(w_x,w_y)$ can be expressed in terms of a 2D sinc function,

$$I_b(f_x,f_y) = \left[\sum_{m\in M}\sum_{n\in N}\exp(-j2\pi(f_x x_m + f_y y_n)) \otimes C_b(f_x,f_y)\right] \times \frac{\sin(\pi f_x w_x)}{\pi f_x w_x}\cdot\frac{\sin(\pi f_y w_y)}{\pi f_y w_y}, \tag{A3}$$

where f_x and f_y are the coordinates corresponding to x and y in the Fourier spatial frequency domain and $C_b(f_x,f_y)$ is the Fourier transform of the binary function $c_b(x_m,y_n)$. Notice that the scaling factors were neglected. The exponential terms in Eq. (A3) account for the phase accumulation dependent on the shift of each pixel relative to the (0, 0) reference position.

The binary image has a resolution of one pixel by construction (the transition from maximum to minimum intensity takes place in one pixel). To modify the resolution and generate the set of templates that are used to correlate with the image under analysis, we implemented a Gaussian filter with a FWHM equal to w_f. These Gaussian filters are used to generate the set of templates with a known resolution. In the spatial frequency domain the Gaussian filter is represented by

$$F(f_x,f_y,w_f) = \exp\left(-\frac{\pi^2 w_f^2}{4\ln 2}(f_x^2+f_y^2)\right). \tag{A4}$$

The effect of reducing the spatial resolution in an image is equivalent to decreasing the range of the spatial frequencies in its Fourier domain. To generate a series of templates with a different spatial resolution, we initially applied the filter defined in Eq. (A4) to each one of the pixels in the binary template described by Eq. (A3). This corresponds in the spatial domain to a convolution, while the spatial frequency domain can be described as the product of the two functions,

$$T(f_x,f_y) = I_b(f_x,f_y)\cdot F(f_x,f_y,w_f), \tag{A5}$$

where $T(f_x,f_y)$ describes the template after applying a filter of width w_f represented in the Fourier domain. We assume that the pixels are squares; this is $w_x=w_y=w_0$. Furthermore, we also replace each square pixel by a Gaussian pixel defined as a Gaussian profile with a FWHM equal to w_0. This substitution modifies the binary template and generates an error that is 6% at the most and can be easily evaluated by comparing the integral of a 2D square function (representing the real square pixel) with the integral of a 2D Gaussian function (representing the approximate Gaussian pixel). The Gaussian pixel provides a convenient way to easily establish an analytical relationship between the Gaussian filter's width and the spatial resolution. The substitution of the square pixels by the Gaussian pixels results in changing the image function defined in Eq. (A3) to

$$I_b(f_x,f_y) = \left[\sum_{m\in M}\sum_{n\in N}\exp(-j2\pi(f_x x_m + f_y y_n)) \otimes C_b(f_x,f_y)\right] \times\exp\left(-\pi^2\frac{w_0^2}{4\ln 2}(f_x^2+f_y^2)\right). \tag{A6}$$

With this substitution Eq. (A5) becomes

$$T(f_x,f_y) = \left[\sum_{m\in M}\sum_{n\in N}\exp(-j2\pi(f_x m\cdot w_0 + f_y n\cdot w_0)) \otimes C_b(f_x,f_y)\right]\exp\left(-\pi^2\frac{w_0^2}{4\ln 2}(f_x^2+f_y^2)\right) \times\exp\left(-\pi^2\frac{w_f^2}{4\ln 2}(f_x^2+f_y^2)\right). \tag{A7}$$

This expression corresponds in the spatial domain to a convolution expressed as

$$t(x,y) = \left[\sum_{m\in M} \sum_{n\in N} \delta(x - m\cdot w_0, y - n\cdot w_0) \cdot C_b(x,y) \right] \otimes \exp\left(- \frac{4\ln 2}{w_0^2}(x^2+y^2) \right) \otimes \exp\left(- \frac{4\ln 2}{w_f^2}(x^2+y^2) \right). \quad \text{(A8)}$$

The first two terms in this expression are the approximated image function $i_b(x_m,y_n)$, where the rectangular pixels have been replaced by the Gaussian pixels of width w_0.

To evaluate the effect of the Gaussian filtering in the Gaussian pixels, let us consider the simplest case of an image composed of only one pixel with a value 1 in the position $m=n=0$. In this simplified example the convolution with a Gaussian filter of width w_f can be expressed by

$$T(f_x,f_y,w_0,w_f) = \exp\left(- \pi^2 \frac{w_0^2 + w_f^2}{4\ln 2}(f_x^2+f_y^2) \right) = \exp\left(- \pi^2 \frac{\delta^2}{4\ln 2}(f_x^2+f_y^2) \right), \quad \text{(A9)}$$

where $\delta=\sqrt{w_0^2+w_f^2}$ is the FWHM of the image obtained after a Gaussian filter of width w_f is applied to a Gaussian pixel of width w_0. This relation shows that applying the Gaussian filter causes the image's features to be larger by a factor $\eta=\delta/w_0$. In the spatial frequency domain this is equivalent to reducing the spectrum width by the same factor. The resolution of the filtered image can thus be related to the factor δ. The width of the filter necessary to apply in reducing the spectrum by a factor η may now be expressed as

$$w_f(\delta) = w_0 \sqrt{\left(\frac{\delta}{w_0}\right)^2 - 1} = w_0\sqrt{\eta^2-1}. \quad \text{(A10)}$$

To improve the sampling in the definition of the filter, in particular when the filter's FWHM becomes comparable to the pixel size, the initial pixel was divided by an integer factor r. This division increases the size of the array containing the image by a factor $r\times r$. The new image represented with the smaller pixels is obtained by extrapolation using the nearest neighborhood method. The extrapolation also changes the scale of the image. The pixel in the expanded scale will have a width $w_0'=w_0/r$. The Gaussian pixel with original width w_0 will be represented by a Gaussian pixel with width $r\cdot w_0'$. All the formalism presented herein now applies to the image with the smaller pixels and the filter width can be expressed as

$$w_f'(\delta) = w_0 \sqrt{\left(\frac{\delta}{w_0/r}\right)^2 - 1} = (w_0'\cdot r)\sqrt{(\eta\cdot r)^2 - 1}. \quad \text{(A11)}$$

Equation (A11) was used to calculate the width of the Gaussian filter that is necessary to apply in obtaining a spectral reduction of a factor η in the filtered image. Although in all this formalism we are approximating the image that originally had square pixels by an image with Gaussian pixels, the approximation gives very good results as was shown in the initial analysis of the images processed with this algorithm. In all the images analyzed, the pixel size was $w_0=12.5$ nm. Using an extrapolation factor $r=5$ in the data processing, the resulting pixel size is $w_0'=2.5$ nm.

ACKNOWLEDGMENTS

This work was supported by the NSF ERC for Extreme Ultraviolet Science and Technology award EEC-0310717. We acknowledge fruitful discussions with M. Azimi-Sadjadi regarding the image processing procedure.

REFERENCES

1. W. L. Chao, B. D. Harteneck, J. A. Liddle, E. H. Anderson, and D. T. Attwood, "Soft x-ray microscopy at a spatial resolution better than 15 nm," Nature **435**, 1210–1213 (2005).
2. P. A. C. Takman, H. Stollberg, G. A. Johansson, A. Holmberg, M. Lindblom, and H. M. Hertz, "High-resolution compact x-ray microscopy," J. Microsc. **226**, 175–181 (2007).
3. G. Vaschenko, C. Brewer, E. Brizuela, Y. Wang, M. A. Larotonda, B. M. Luther, M. C. Marconi, J. J. Rocca, and C. S. Menoni, "Sub-38 nm resolution tabletop microscopy with 13 nm wavelength laser light," Opt. Lett. **31**, 1214–1216 (2006).
4. H. M. Hertz, G. A. Johansson, H. Stollberg, J. de Groot, O. Hemberg, A. Holmberg, S. Rehbein, P. Jansson, F. Eriksson, and J. Birch, "Tabletop x-ray microscopy: sources, optics and applications," J. Phys. IV **104**, 115–119 (2003).
5. D. Attwood, *Soft X-Ray and Extreme Ultraviolet Radiation, Principles and Applications* (Cambridge U. Press, 2000), p. 357.
6. J. Heck, D. T. Attwood, W. Meyer-Ilse, and E. H. Anderson, "Resolution determination in x-ray microscopy: an analysis of the effects of partial coherence and illumination spectrum," J. X-Ray Sci. Technol. **8**, 95–104 (1998).
7. Q. Kemao, "Two-dimensional windowed Fourier transform for fringe pattern analysis: principles, applications and implementations," Opt. Lasers Eng. **45**, 304–317 (2007).
8. M. S. Pattichis and A. C. Bovik, "Analyzing image structure by multidimensional frequency modulation," IEEE Trans. Pattern Anal. Mach. Intell. **29**, 753–766 (2007).
9. H. Stollberg, J. B. De Monvel, A. Holmberg, and H. M. Hertz, "Wavelet-based image restoration for compact x-ray microscopy," J. Microsc. **211**, 154–160 (2003).
10. H. Stollberg, P. Guttmann, P. A. C. Takman, and H. M. Hertz, "Size-selective colloidal-gold localization in transmission x-ray microscopy," J. Microsc. **225**, 80–87 (2007).
11. P. Wachulak, M. C. Marconi, R. Bartels, C. S. Menoni, and J. J. Rocca, "Volume extreme ultraviolet holographic imaging with numerical optical sectioning," Opt. Express **15**, 10622–10628 (2007).
12. J. Nunez, X. Otazu, and M. T. Merino, "A multiresolution-based method for the determination of the relative resolution between images: first application to remote sensing and medical images," Int. J. Imaging Syst. Technol. **15**, 225–235 (2005).
13. P. Wachulak, R. Bartels, M. C. Marconi, C. S. Menoni, J. J. Rocca, Y. Lu, and B. Parkinson, "Sub 400 nm spatial resolution extreme ultraviolet holography with a table top laser," Opt. Express **14**, 9636–9642 (2006).
14. Y. Wang, M. A. Larotonda, B. M. Luther, D. Alessi, M. Berrill, V. N. Shlyaptsev, and J. J. Rocca, "Demonstration of high-repetition-rate tabletop soft-x-ray lasers with

saturated output at wavelengths down to 13.9 nm and gain down to 10.9 nm," Phys. Rev. A **72**, 053807 (2005).
15. J. J. Rocca, Y. Wang, M. A. Larotonda, B. M. Luther, M. Berrill, and D. Alessi, "Saturated 13.2 nm high-repetition-rate laser in nickellike cadmium," Opt. Lett. **30**, 2581–2583 (2005).
16. E. H. Anderson, "Specialized electron beam nanolithography for EUV and x-ray diffractive optics," IEEE J. Quantum Electron. **42**, 27–35 (2006).
17. E. H. Anderson, D. L. Olynick, B. Harteneck, E. Veklerov, G. Denbeaux, W. L. Chao, A. Lucero, L. Johnson, and D. Attwood, "Nanofabrication and diffractive optics for high-resolution x-ray applications," J. Vac. Sci. Technol. B **18**, 2970–2975 (2000).
18. T. Yatagai, S. Nakadate, M. Idesawa, and H. Saito, "Automatic fringe analysis using digital image processing techniques," Opt. Eng. (Bellingham) **21**, 432–435 (1982).